

Correlated Particle Motion and THz Spectral Response of Supercritical Water

Maciej Śmiechowski*

*Department of Physical Chemistry, Chemical Faculty,
Gdańsk University of Technology, Narutowicza 11/12, 80-233 Gdańsk, Poland and
Lehrstuhl für Theoretische Chemie, Ruhr-Universität Bochum, 44780 Bochum, Germany*

Christoph Schran, Harald Forbert, and Dominik Marx

*Lehrstuhl für Theoretische Chemie, Ruhr-Universität Bochum, 44780 Bochum, Germany
(Dated: February 2, 2022)*

Molecular dynamics simulations of supercritical water reveal distinctly different distance-dependent modulations of dipolar response and correlations in particle motion compared to ambient conditions. The strongly perturbed H-bond network of water at supercritical conditions allows for considerable translational and rotational freedom of individual molecules. These changes give rise to substantially different infrared spectra and vibrational density of states at THz frequencies for densities above and below the Widom line that separates percolating liquid-like and clustered gas-like supercritical water.

PACS numbers: 61.20.Ja, 78.30.C-, 78.15.+e, 82.30.Rs

Supercritical matter is an ideal testing ground to systematically study fundamental aspects of fluids as a function of density [1–8]. Although formally being single phase systems, supercritical fluids nevertheless show two distinct regions that are separated by the so-called Widom line, distinguishing gas-like and liquid-like dynamical regimes that are reminiscent of the respective subcritical domains [3, 4, 6–8]. Hence, supercritical fluids are not only far more complex in nature than believed for a long time, but the distinct regimes also encompass vastly different properties. Transcending fundamentals, the study of liquids above their critical point (CP) is also motivated by their increasing importance for large-scale industrial processes, serving e.g. as environmentally friendly “green solvents” [9, 10].

Most notably supercritical water (SCW; CP: $T_c = 647$ K, $p_c = 22.1$ MPa, $\rho_c = 0.32$ g/cm³) becomes an increasingly important processing medium for key transformations in benign aqueous environments [11]. The latter owes much to the dramatically reduced dielectric constant of SCW (from ~ 80 at ambient conditions to ~ 6 just above the CP) [12]. On the other hand, SCW becomes fairly conducting up to the point of metalizing above 7000 K in the GPa pressure range [13]. All this makes SCW a “tunable fluid environment” with amazing properties [14]. The macroscopic phenomena that underlie these peculiarities at the microscopic level seem to be driven chiefly by significant changes in the hydrogen bond (H-bond) network of water at extreme conditions. Such structure of SCW is well-studied using neutron/x-ray diffraction (ND/XRD) [15–17], quasi-elastic neutron scattering (QENS) [18] with energy transfers up to 100 meV (≈ 800 cm⁻¹) and deep inelastic neutron (Compton)/x-ray (Raman) scattering (DINS/IXS) [19–21] in the eV range, thus spanning many orders of magnitude in time but also in length scales depending

on momentum transfer. For instance, the dynamic structure factor obtained from incoherent QENS of SCW [18] yields, in the limit $Q < 1$ Å⁻¹, the density of states of H atoms up to ca. 800 cm⁻¹ (≈ 24 THz). Complementing structure, dynamic relaxation [22] of SCW has been probed as well by NMR.

Experiments on SCW can be interpreted at the molecular level by analyzing molecular dynamics (MD) simulations that can be directly compared with experimental data [23]. The electronic structure of SCW is accessible via ab initio MD (AIMD) [24] that allow one to compute dipole moments and vibrational spectra [25] as well as IXS spectra [21]. Moreover, AIMD simulations also provide computational access to reactions in SCW [26].

When it comes to elucidating H-bond dynamics, infrared (IR) spectroscopy remains the prime technique to study water [27] including SCW [28, 29]. IR spectroscopy is sensitive primarily to atomic and/or molecular motion that gives rise to dipole moment changes along the associated oscillatory displacements [30]. Upon lowering the frequency, i.e. the excitation energy, one can successively probe fast intramolecular vibrations in the 4000–500 cm⁻¹ (120–15 THz) mid-IR range, intermolecular dynamics such as H-bond motion or hindered molecular rotations and translations in the 500–50 cm⁻¹ (15–1.5 THz) far-IR regime [30], and even slower phenomena such as dielectric relaxation at GHz frequencies [31], thus allowing one to probe specific processes on their intrinsic timescales. Vibrational spectroscopy of water in the *mid-IR regime* is particularly sensitive to cluster size, H-bond abundance and H-bond strength as the *intramolecular* stretching band of H₂O is the traditional probe of these [28, 29, 32]. In recent years, however, the *far-IR region* of the vibrational spectrum, now commonly referred to as the “terahertz” (THz) regime (note that 100 cm⁻¹ ≈ 3 THz ≈ 12 meV), has been appreciated

to offer direct insights into the picosecond dynamics — and thus into *intermolecular* motion such as H-bond network dynamics being characteristic to liquid water. Advances in THz laser spectroscopy closed the “THz gap” in IR spectroscopy and now permit unprecedented insights for instance into the modified H-bond dynamics in the vicinity of molecules [33–35]. For ambient water, it has been shown theoretically that THz spectroscopy indeed probes specific intermolecular modes of the H-bond network [36]. For aqueous solutions of simple ions, the THz response due to these perturbations has been computed [37, 38] and THz peaks could even be assigned to distinct intermolecular modes in the case of molecules [39].

In this Letter we investigate — with a clear focus on changes of the THz spectral response — the properties of water at two supercritical state points that represent gas-like and liquid-like H-bond dynamics in the spirit of Widom crossover. We uncover to what extent the dramatic changes in the dynamical H-bond network fluctuations associated with crossing the percolation line affect cross-correlations in particle motion in a spatially-resolved frequency-domain picture, and how the intermolecular dipolar correlations of supercritical fluids qualitatively change their THz responses compared to ambient water.

For this study we selected two supercritical state points (at $T = 660$ K) located deep in the two regimes separated by the Widom line [6] (and by the percolation line of SCW [17]), namely at $\rho = 0.2$ g/cm³ (low-density, LD-SCW) and at 0.6 g/cm³ (high-density, HD-SCW). For reference, we also performed ambient condition simulations at 300 K and 0.997 g/cm³ (room-temperature water, RTW). It is noted in passing that we must resort to force field MD (see Supplemental Material, SM [40]) in order to provide the statistical data base that allows us to spatially decompose the long-ranged intermolecular dependencies at THz frequencies. As a first test of the adequacy of these simulations, we investigate the global structure of SCW as revealed by $g_{OO}(r)$ in Fig. 1. These radial distribution functions (RDFs) compare most favorably with the available experimental data at matching densities (0.23 g/cm³ [52] and 0.58 g/cm³ [17]) as do the corresponding O–H and H–H correlations [40].

The corresponding microscopic structure is reflected in the H-bonding properties of the fluids. In contrast to RTW, where essentially all molecules form an interconnected three-dimensional H-bond network, SCW is characterized by the appearance of isolated patches (“clusters”) that fluctuate rapidly on a (sub-)picosecond time scale [53]. The lifetime of these clusters is of course somewhat dependent on the applied H-bond definition [54] and we follow here a variant of the standard geometric criterion [40].

In Fig. 2 we analyze the clustering properties of SCW at the two state points compared to RTW. While for

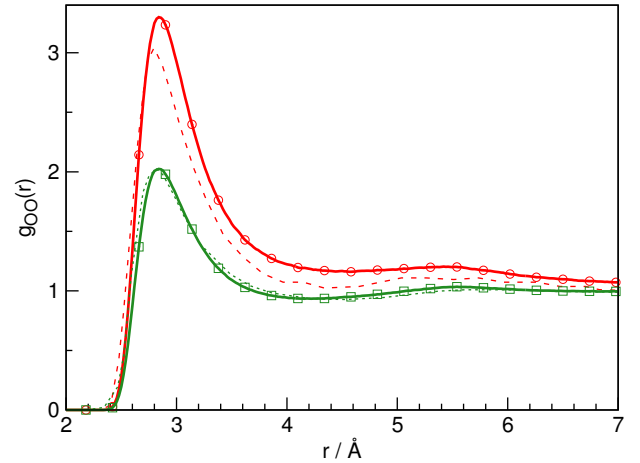


Figure 1. Radial distribution functions $g_{OO}(r)$ for LD-SCW (red line with circles) and HD-SCW (green line with squares) compared to experimental data at $\rho = 0.23$ g/cm³ (Ref. 52, dashed line) and 0.58 g/cm³ (Ref. 17, dotted line).

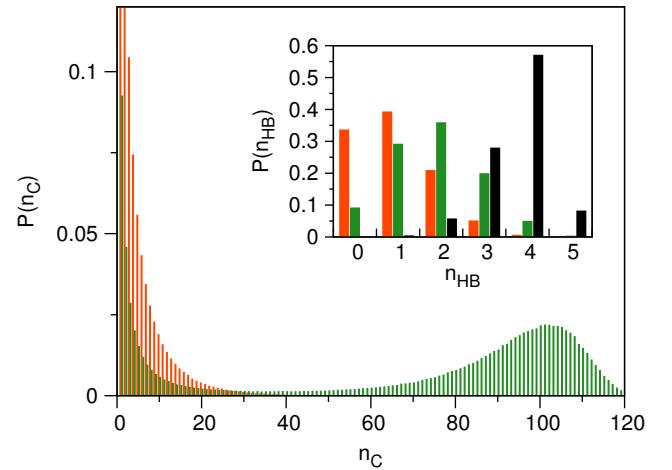


Figure 2. Probability that a water molecule belongs to a cluster of size n_C for LD-SCW (red, where $P(n_C = 1) = 34\%$ and $P(2) = 17\%$) and HD-SCW (green). The inset shows the distribution of the water molecules according to the number of H-bonds formed including RTW (black).

LD-SCW the relative abundance of the clusters decays almost exponentially with the cluster size, having highest values for water monomers followed by dimers, the distribution for HD-SCW is clearly bimodal with one maximum at non-H-bonded individual molecules and another one close to the total available number of water molecules; these $P(n_C)$ distributions are in good agreement with previous simulations [53]. In the inset of Fig. 2 the propensity of the water molecules to form H-bonds is illustrated. For LD-SCW, non-H-bonded and singly H-bonded molecules predominate, while this shifts to singly and doubly H-bonded ones at the higher den-

sity. Importantly, the H-bond statistics in both cases is markedly different from RTW, where four-coordinated molecules form a dense network (i.e. a single “cluster” so that $P(n_C = 128) \approx 1$) and $\langle n_{HB} \rangle = 3.68 \pm 0.07$. For comparison: $\langle n_{HB} \rangle = 1.84 \pm 0.11$ and 1.00 ± 0.12 for HD- and LD-SCW, respectively, in agreement with other simulations [54, 55]. We checked on larger systems that these conclusions are stable when increasing the system size [40]. An independent experimental confirmation of the dramatic reduction of H-bonding in SCW comes from the Compton profiles obtained from IXS [19] that provide indirect access to $\langle n_{HB} \rangle$ via the number of electrons involved in hydrogen bonding. The $\langle n_{HB} \rangle$ value is then found to decrease from 3.40 for RTW to 0.73 for SCW (at $\rho = 0.4 \text{ g/cm}^3$ and 670 K) [19] in agreement with our findings.

The significant changes in the fluid structure of SCW are expected to alter significantly its IR spectrum [28, 29]. Particularly in the THz range, being utmost sensitive to H-bond dynamics, temperature increase is known to lead to major changes as observed experimentally already at *subcritical* conditions. Below the CP, the two main features of the RTW spectrum, that is the librational mode at $\approx 680 \text{ cm}^{-1}$ ($\approx 20 \text{ THz}$) and the intermolecular H-bond stretching mode at $\approx 200 \text{ cm}^{-1}$ (6 THz), are known to merge gradually into a single feature centered at $\approx 450 \text{ cm}^{-1}$ ($\approx 13.5 \text{ THz}$) upon increasing the temperature to 510 K along the gas-liquid coexistence curve [28]; note that SCW spectra in the THz range have not yet been measured.

Our THz spectra computed [40] from the Fourier transform of the dipole derivative time correlation function (TCF) are shown in Fig. 3. It is well known that flexible force fields without polarizability and/or charge transfer cannot reproduce the THz spectra of RTW, in particular not the eminent H-bond network mode at $\approx 200 \text{ cm}^{-1}$ (6 THz). Several schemes to correct for this deficiency have been proposed and both so-called “Torii corrections” [56, 57] reach a considerable agreement with experimental and AIMD IR spectra of RTW [36]. In Torii’s schemes, which we generalized in the SM [40] to flexible water models, polarization effects due to H-bonding are incorporated. In the more advanced version [57], this is achieved by adding both intermolecular charge fluxes to existing H-bonds and local electric field effects to each molecule when computing the total dipole moment according to Eqs. (S25)–(S28). We scrutinized [40] the applicability of these corrections to SCW and conclude that they can be neglected in this regime, which is backed up by comparison to available spectra (see Sec. IV.E and Fig. S7 [40]), in stark contrast to RTW. The THz spectra obtained with the most recent Torii correction [57] as well as the uncorrected original spectra clearly illustrate this point, see Fig. 3.

In the supercritical regime the THz lineshape function changes dramatically compared to ambient conditions:

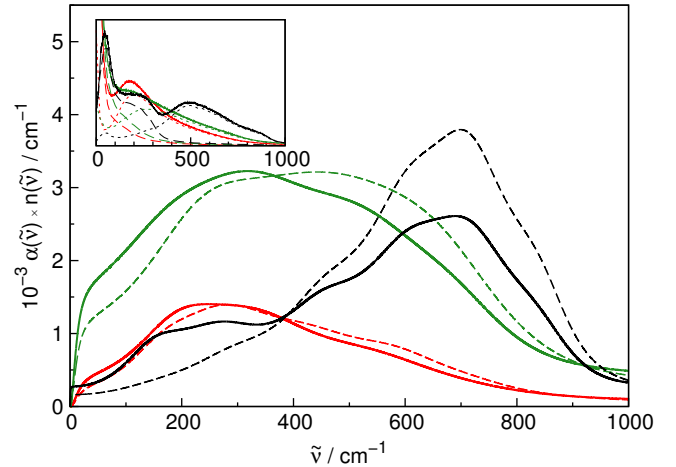


Figure 3. Computed total THz absorption spectra of water at the LD-SCW (red), HD-SCW (green), and RTW (black) state points. The Torii-corrected [57] spectra (solid lines) are compared to the uncorrected spectra (dashed lines), see text. The inset shows the corresponding vibrational density of states with separate contributions due to O (dashed lines) and H (dotted lines) atoms. The zero-frequency peak of LD- and HD-SCW is off scale and the data are magnified in Fig. S4 [40].

it becomes unimodal in the first place and centered at roughly 300 cm^{-1} (9 THz) at high density, while for LD-SCW it shifts down to about 200 cm^{-1} (6 THz) according to Fig. 3. Even more pronounced are the changes in the vibrational density of states (VDOS), see the inset or Fig. S4 [40]. The librational band at $\approx 500 \text{ cm}^{-1}$ (15 THz) disappears for SCW in both the gas-like and liquid-like dynamical regimes, while the principal peak due to the oxygen atoms movement at $< 100 \text{ cm}^{-1}$ ($< 3 \text{ THz}$) shifts to zero frequency and dramatically increases in intensity, reflecting the only slightly hindered *translational* (“ballistic”) movement of water molecules in the supercritical fluid. The latter is also evident from the value of the self-diffusion coefficient estimated via the Green-Kubo relation from the center-of-mass velocity TCF. It increases from 0.23 for RTW to 4.92 for HD-SCW to $14.17 \text{ \AA}^2/\text{ps}$ for LD-SCW in accordance with the available QENS data [18] (7.65 and $13.70 \text{ \AA}^2/\text{ps}$, respectively). Considering separately the O/H atoms VDOS (as defined in Sec. III of the SM [40]), the strikingly changing nature of the $\approx 200 \text{ cm}^{-1}$ (6 THz) band is revealed. While in RTW it is mainly due to oxygen motion, in SCW it is the hydrogen motion that underlies this vibrational activity due to much more *rotational* freedom of the individual water molecules. This already gives a glimpse into the fundamentally different nature of this resonance at supercritical versus ambient conditions, *vide infra*.

The intra- and intermolecular correlations underlying both the IR spectra and VDOS can be resolved when applying a spatial decomposition scheme [36]. To this

end, either molecular dipole velocities or mass-weighted atomic velocities are projected on a grid to obtain spatially resolved charge current or mass-weighted velocity density vector fields which are then auto-correlated [40]. For isotropic liquids, such as RTW and SCW, angular averaging leaves only a radial dependence of the spectrum, at each frequency, on the distance from the reference point. The resulting radially-resolved spectral response might be understood most easily in analogy to RDFs: while the latter describe radial correlations *in particle density* with increasing separation r , the former captures *vibrational correlations* (in IR or particle dynamics) in a similar manner.

The radially-resolved IR spectra of water reveal in the THz spectral range a characteristic loss of spatial correlations with decreasing density, see panels **a–c** of Fig. 4. While for RTW, dipolar correlations up to the second hydration sphere are clearly detectable in qualitative agreement with previous AIMD analyses [36], for HD-SCW only the cross-correlations within the first hydration sphere at roughly 3 Å are important. Even these short-range correlations fade away upon further expansion of supercritical water to LD conditions. For LD-SCW, the major correlation features at this distance become less intense and steadily red-shift relative to RTW by as much as 250 cm⁻¹. Such red-shifts of the positive and negative *cross-correlation* peaks reflect the increased librational freedom of the water molecules in the supercritical state due to the lower degree of H-bonding upon decreasing the density. This general trend is in line with what has been observed in the *subcritical* regime [28] upon raising the temperature.

In the *supercritical* regime, our findings therefore extend the Widom line crossover concept from thermodynamics and dynamics [3, 4, 6] now into correlated dipolar response and THz vibrational spectra. The presence of weak correlations in the radially-resolved spectra of SCW suggests that some nearest-neighbor dipolar couplings are still effective even in supercritical water, while the long-range correlations are strongly suppressed in the LD-SCW case due to the completely disrupted tetrahedral H-bond network of water. This directly relates the THz response of gas-like and liquid-like SCW to the percolation line [17].

Contrasting next the radially-resolved vibrational correlations (see panels **d–f** in Fig. 4) to the dipolar THz response (panels **a–c**) it is striking to find out that the distinctly modulated pattern characteristic for RTW becomes greatly simplified at supercritical conditions. With reference to RTW [36], this implies for SCW the progressively diminishing spatial range and magnitude of cross-correlations of the H-bond umbrella motion at ca. 80 cm⁻¹ (2.4 THz), H-bond network stretching at 200 cm⁻¹ (6 THz), librations at roughly 500 cm⁻¹ (15 THz), as well as the absence of any noteworthy correlations in the intramolecular vibrations range at still

higher (mid-IR) frequencies. This reflects the radical changes in the nature of the underlying atomic motion at supercritical compared to ambient conditions. The steeply rising positive correlations close to zero frequency can be attributed to increasingly “ballistic” movement of those water molecules which are no longer firmly engaged in an extended H-bond network in SCW. This pseudo-hard sphere character of water molecules in SCW and the long-range nature of the observed velocity cross-correlations are reminiscent of the similarly far-reaching correlations in the sedimentation of colloidal particles due to instantaneous density fluctuations [58]. Next, the weak and broad feature at 200–300 cm⁻¹ does not show much correlations even with nearest-neighbor molecules (expected at $r \approx 3$ Å), but instead it is due to single-molecule motion (visible at $r \approx 0$ Å) mainly of H atoms (see Fig. S4 in the SM [40]). This librational single-particle motion is distinctly different from the “network mode” of RTW at 200 cm⁻¹ (6 THz) that is caused by intermolecular stretching motion of tetrahedrally H-bonded water molecules [36] as evidenced by the prominent cross-correlations at $r \approx 3$ Å (panel **f** in Fig. 4). Our peak assignment of the spectra in Figs. 4 and 3 is strongly supported by QENS experiments [18] which provide a DOS for protons (see Fig. 9 therein) that features a clearly structured response with two pronounced maxima at roughly 60 and 520 cm⁻¹ (7 and 65 meV) for RTW, while only one broad unimodal resonance is observed for HD-SCW (at $\rho = 0.59$ g/cm³ and 653 K) close to 240 cm⁻¹ (≈ 30 meV). This nicely agrees with our partial VDOS for H atoms as depicted in Fig. S4 [40] with two peaks at about 45 and 500 cm⁻¹ for RTW and a single broadband feature at 275 cm⁻¹ for HD-SCW.

In conclusion, dramatic changes of the THz response of supercritical water are predicted in this spectral region characteristic of the tetrahedral H-bond network of liquid water, which are traced back to significantly decreasing long-range intermolecular correlations. In particular, the celebrated “network mode” of ambient water at around 200 cm⁻¹ (6 THz) vanishes at supercritical conditions, while the libration band red-shifts by as much as 250 cm⁻¹. Thus, instead of being bimodal, the supercritical THz spectra show a single but unusually broad, mainly librational feature around 200–300 cm⁻¹. Understanding the molecular mechanism that leads to the observed THz resonances will be key to interpret future experiments of supercritical water and solutions. In particular, the far-reaching couplings characteristic to the THz response of ambient liquid water are found to be suppressed when crossing the percolation line by moving from high to low densities and thus from liquid-like to gas-like supercritical water, respectively. The associated changes of the H-bond network motion across the Widom line are encoded in changes of the correlated dipolar response as probed by THz vibrational spectroscopy, which therefore complements thermodynamic and dy-

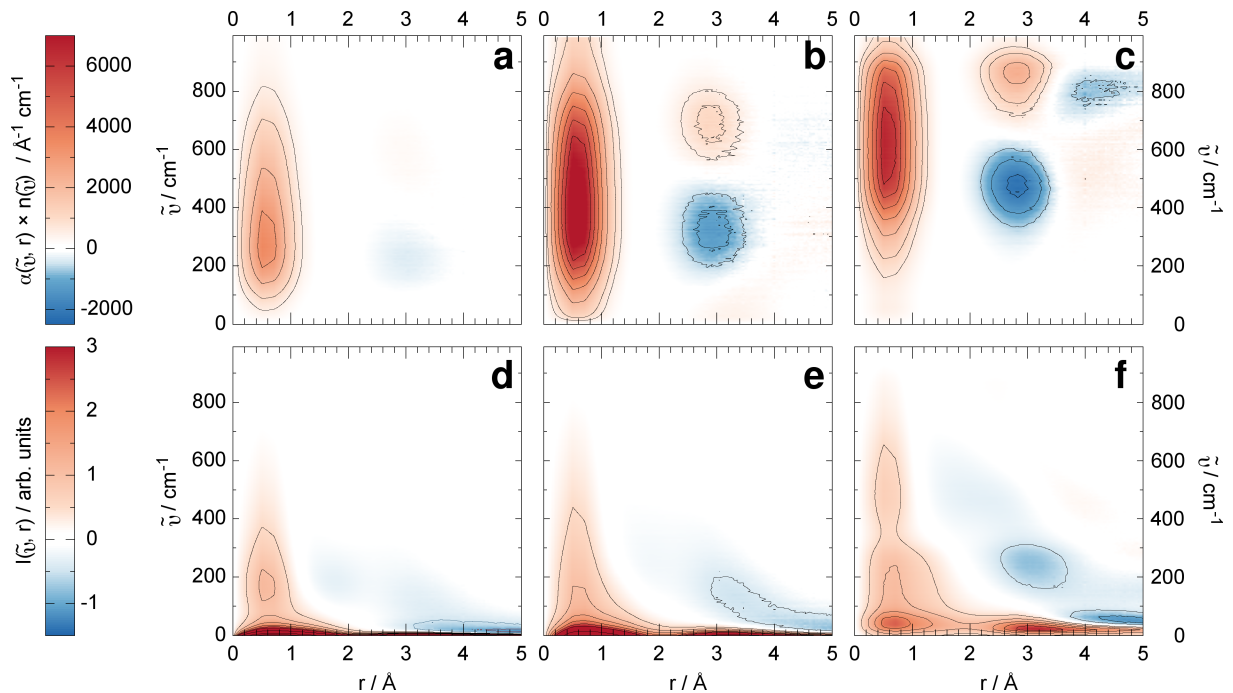


Figure 4. Top: Radially-resolved THz absorption spectra of water at the (a) LD-SCW, (b) HD-SCW, and (c) RTW state points. Bottom: Corresponding radially-resolved vibrational correlations (“generalized VDOS”) at the (d) LD-SCW, (e) HD-SCW, and (f) RTW state points. Figure S8 provides a three-dimensional representation of the same data [40].

dynamic techniques to investigate this crossover concept in supercritical water and beyond. Finally, THz spectroscopy with its ability to detect changes in the H-bond network between high- and low-density water might be an ideal technique to also shed light on the Widom line in the framework of the controversially discussed (second) liquid-liquid critical point of supercooled water.

We are particularly grateful to Hajime Torii for clarifying the details of his IR corrections. We acknowledge partial financial support from DFG (MA 1547/11 and Cluster of Excellence “RESOLV” EXC 1069). Computations were performed at LRZ München, HPC-RESOLV@RUB, BOVILAB@RUB, and RV-NRW.

* Corresponding author. Electronic mail: Maciej.Smiechowski@pg.gda.pl

- [1] A. Cunsolo, G. Pratesi, G. Ruocco, M. Sampoli, F. Sette, R. Verbeni, F. Barocchi, M. Krisch, C. Masciovecchio, and M. Nardone, *Phys. Rev. Lett.* **80**, 3515 (1998).
- [2] F. Gorelli, M. Santoro, T. Scopigno, M. Krisch, and G. Ruocco, *Phys. Rev. Lett.* **97**, 245702 (2006).
- [3] G. G. Simeoni, T. Bryk, F. A. Gorelli, M. Krisch, G. Ruocco, M. Santoro, and T. Scopigno, *Nat. Phys.* **6**, 503 (2010).
- [4] P. F. McMillan and H. E. Stanley, *Nat. Phys.* **6**, 479 (2010).
- [5] D. Bolmatov, V. Brazhkin, and K. Trachenko, *Nat. Commun.* **4**, 2331 (2013).
- [6] P. Gallo, D. Corradini, and M. Rovere, *Nat. Commun.* **5**, 5806 (2014).
- [7] V. P. Sokhan, A. Jones, F. S. Cipcigan, J. Crain, and G. J. Martyna, *Phys. Rev. Lett.* **115**, 117801 (2015).
- [8] Y. D. Fomin, V. N. Ryzhov, E. N. Tsiok, and V. V. Brazhkin, *Sci. Rep.* **5**, 14234 (2015).
- [9] C.-J. Li and B. M. Trost, *Proc. Natl. Acad. Sci. U. S. A.* **105**, 13197 (2008).
- [10] J. M. DeSimone, *Science* **297**, 799 (2002).
- [11] P. G. Jessop, T. Ikariya, and R. Noyori, *Science* **269**, 1065 (1995).
- [12] D. Pan, L. Spanu, B. Harrison, D. A. Sverjensky, and G. Galli, *Proc. Natl. Acad. Sci. U. S. A.* **110**, 6646 (2013).
- [13] C. Cavazzoni, G. L. Chiarotti, S. Scandolo, E. Tosatti, M. Bernasconi, and M. Parrinello, *Science* **283**, 44 (1999).
- [14] H. Weingärtner and E. U. Franck, *Angew. Chem. Int. Ed.* **44**, 2672 (2005).
- [15] P. Postorino, R. H. Tromp, M.-A. Ricci, A. K. Soper, and G. W. Neilson, *Nature* **366**, 668 (1993).
- [16] H. Ohtaki, T. Radnai, and T. Yamaguchi, *Chem. Soc. Rev.* **26**, 41 (1997).
- [17] M. Bernabei, A. Botti, F. Bruni, M.-A. Ricci, and A. K. Soper, *Phys. Rev. E* **78**, 021505 (2008).
- [18] T. Tassaing and M.-C. Bellissent-Funel, *J. Chem. Phys.* **113**, 3332 (2000).
- [19] P. H.-L. Sit, C. Bellin, B. Barbiellini, D. Testemale, J.-L. Hazemann, T. Buslaps, N. Marzari, and A. Shukla, *Phys. Rev. B* **76**, 245413 (2007).
- [20] C. Pantalei, A. Pietropaolo, R. Senesi, S. Imberti, C. Andreani, J. Mayers, C. Burnham, and G. Reiter, *Phys. Rev. Lett.* **100**, 177801 (2008).
- [21] C. J. Sahle, C. Sternemann, C. Schmidt, S. Lehtola,

- S. Jahn, L. Simonelli, S. Huotari, M. Hakala, T. Pylkkanen, A. Nyrow, K. Mende, M. Tolan, K. Hamalainen, and M. Wilke, *Proc. Natl. Acad. Sci. U. S. A.* **110**, 6301 (2013).
- [22] N. Matubayasi, C. Wakai, and M. Nakahara, *Phys. Rev. Lett.* **78**, 2573 (1997).
- [23] A. G. Kalinichev, *Rev. Mineral. Geochem.* **42**, 83 (2001).
- [24] D. Marx and J. Hutter, *Ab Initio Molecular Dynamics* (Cambridge University Press, Cambridge, 2009).
- [25] M. Boero, K. Terakura, T. Ikeshoji, C. C. Liew, and M. Parrinello, *Phys. Rev. Lett.* **85**, 3245 (2000).
- [26] M. Boero, M. Parrinello, K. Terakura, T. Ikeshoji, and C. C. Liew, *Phys. Rev. Lett.* **90**, 226403 (2003).
- [27] T. Yagasaki and S. Saito, *Annu. Rev. Phys. Chem.* **64**, 55 (2013).
- [28] T. Tassaing, Y. Danten, and M. Besnard, *J. Mol. Liq.* **101**, 149 (2002).
- [29] A. Kandratsenka, D. Schwarzer, and P. Vöhringer, *J. Chem. Phys.* **128**, 244510 (2008).
- [30] J. M. Chalmers and P. R. Griffiths, eds., *Handbook of Vibrational Spectroscopy*, Vol. 1. Theory and Instrumentation (John Wiley & Sons, Ltd, 2006).
- [31] C. Rønne, P.-O. Åstrand, and R. S. Keiding, *Phys. Rev. Lett.* **82**, 2888 (1999).
- [32] U. Buck and F. Huiskens, *Chem. Rev.* **100**, 3863 (2000).
- [33] U. Heugen, G. Schwaab, E. Bründermann, M. Heyden, X. Yu, D.-M. Leitner, and M. Havenith, *Proc. Natl. Acad. Sci. U.S.A.* **103**, 12301 (2006).
- [34] S. Ebbinghaus, S.-J. Kim, M. Heyden, X. Yu, U. Heugen, M. Gruebele, D.-M. Leitner, and M. Havenith, *Proc. Natl. Acad. Sci. U.S.A.* **104**, 20749 (2007).
- [35] K. J. Tielrooij, R. L. A. Timmer, H. J. Bakker, and M. Bonn, *Phys. Rev. Lett.* **102**, 198303 (2009).
- [36] M. Heyden, J. Sun, S. Funkner, G. Mathias, H. Forbert, M. Havenith, and D. Marx, *Proc. Natl. Acad. Sci. U.S.A.* **107**, 12068 (2010).
- [37] M. Śmiechowski, H. Forbert, and D. Marx, *J. Chem. Phys.* **139**, 014506 (2013).
- [38] M. Śmiechowski, J. Sun, H. Forbert, and D. Marx, *Phys. Chem. Chem. Phys.* **17**, 8323 (2015).
- [39] J. Sun, G. Niehues, H. Forbert, D. Decka, G. Schwaab, D. Marx, and M. Havenith, *J. Am. Chem. Soc.* **136**, 5031 (2014).
- [40] See Supplemental Material, which includes Refs. 41–51, for additional data, analyses, and computational details.
- [41] K. Toukan and A. Rahman, *Phys. Rev. B* **31**, 2643 (1985).
- [42] A. P. Lyubartsev and A. Laaksonen, *Comp. Phys. Commun.* **128**, 565 (2000).
- [43] G. Raabe and R. J. Sadus, *J. Chem. Phys.* **126**, 044701 (2007).
- [44] A. Luzar and D. Chandler, *Phys. Rev. Lett.* **76**, 928 (1996).
- [45] R. Kumar, J. R. Schmidt, and J. L. Skinner, *J. Chem. Phys.* **126**, 204107 (2007).
- [46] R. Ramírez, T. López-Ciudad, P. Kumar, and D. Marx, *J. Chem. Phys.* **121**, 3973 (2004).
- [47] S. D. Ivanov, A. Witt, and D. Marx, *Phys. Chem. Chem. Phys.* **15**, 10270 (2013).
- [48] M. Heyden, J. Sun, H. Forbert, G. Mathias, M. Havenith, and D. Marx, *J. Phys. Chem. Lett.* **3**, 2135 (2012).
- [49] R. Jonchiere, A. P. Seitsonen, G. Ferlat, A. M. Saitta, and R. Vuilleumier, *J. Chem. Phys.* **135**, 154503 (2011).
- [50] M. S. Skaf and D. Laria, *J. Chem. Phys.* **113**, 3499 (2000).
- [51] B. D. Bursulaya and H. J. Kim, *J. Chem. Phys.* **110**, 9656 (1999).
- [52] M.-C. Bellissent-Funel, T. Tassaing, H. Zhao, D. Beysens, B. Guillot, and Y. Guissani, *J. Chem. Phys.* **107**, 2942 (1997).
- [53] S. V. Churakov and A. G. Kalinichev, *J. Struct. Chem.* **40**, 548 (1999).
- [54] A. G. Kalinichev and J. D. Bass, *Chem. Phys. Lett.* **231**, 301 (1994).
- [55] H. Ma and J. Ma, *J. Chem. Phys.* **135**, 054504 (2011).
- [56] H. Torii, *J. Phys. Chem. B* **115**, 6636 (2011).
- [57] H. Torii, *J. Chem. Theory Comput.* **10**, 1219 (2014).
- [58] P. N. Segrè, E. Herbolzheimer, and P. M. Chaikin, *Phys. Rev. Lett.* **79**, 2574 (1997).